DE GRUYTER OPEN

Archives of Hydro-Engineering and Environmental Mechanics
Vol. 63 (2016), No. 2–3, pp. 173–190
DOI: 10.1515/heem-2016-0011

Rayleigh Waves Transformation in Liquefying Water-saturated Sands

Ryszard Staroszczyk

Institute of Hydro-Engineering, Polish Academy of Sciences, Kościerska 7, 80-328 Gdańsk, Poland,
e-mail: rstar@ibwpan.gda.pl

(Received November 30, 2016; revised January 10, 2017)

Abstract

The behaviour of a water-saturated sand deposit subjected to dynamic loads induced by the propagation of Rayleigh surface waves is analysed. Cyclic shearing of the saturated sand matrix due to ground motions results in the development of excess pore pressures in the soil and its subsequent liquefaction. The phenomena of pore pressure generation and soil liquefaction are investigated within the framework of a compaction theory for saturated granular media. The results of calculations, carried out by a finite-element method, illustrate the evolution of pore pressures and the development of liquefaction zones in the soil, and show the variation of surface wave parameters with the progressive degradation of the strength of the subsoil.

Key words: Rayleigh surface wave, water-saturated sand, excess pore pressure generation, soil liquefaction.

List of symbols

a, b	–	finite element length and height;
a_0^V	–	initial free-surface vertical acceleration amplitude;
c_R	–	Rayleigh wave phase velocity;
D_1, D_2	–	material constants;
$\boldsymbol{e}$	–	infinitesimal strain tensor;
$\boldsymbol{E}$	–	strain amplitude tensor;
G, G_0, G_1	–	shear moduli;
H	–	computational layer depth;
i	–	imaginary unit;
$\boldsymbol{I}$	–	unit tensor;
k	–	Rayleigh wave number;
k_f	–	filtration coefficient;
$\boldsymbol{K}$	–	global stiffness matrix;
L_R	–	Rayleigh wave length;
m	–	number of discrete sublayers along the depth;

$\boldsymbol{M}$ – global mass matrix;
n – volume porosity;
N – number of loading cycles;
p' – mean effective stress;
p^f – pore pressure;
$\boldsymbol{q}$ – global displacement amplitude vector;
s – excess pore pressure;
t – time;
$\boldsymbol{u}$ – soil displacement vector;
U, W – horizontal and vertical displacement amplitudes;
x, z – Cartesian coordinates;
κ – soil skeleton compressibility;
λ – Lamé's elastic constant;
ρ – mass density;
$\boldsymbol{\sigma}$ – stress tensor;
$\boldsymbol{\sigma}^f, \boldsymbol{\sigma}^s$ – partial stress tensors in pore fluid and sand skeleton;
Φ – sand compaction parameter;
ω – angular frequency.

1. Introduction

Although the mechanism of soil liquefaction has already been known for about a century, it attracted closer attention from scientists and engineers only after the 1964 Niigata and 1964 Alaska earthquakes, during which the effects of the soil liquefaction on civil infrastructure were devastating. Serious laboratory research then started, and first theoretical models describing the phenomenon of soil liquefaction were formulated within a decade (Seed and Lee 1966, Seed and Peacock 1971, Finn et al 1971, Martin et al 1975, Finn et al 1977). Most of these early efforts were concentrated in the USA, though soon the interests in this topic spread to research centres in other countries, and the number of scientists contributing to this research field gradually increased.

One of the leading contributors to the field was Prof. A. Sawicki from the Institute of Hydro-Engineering of the Polish Academy of Sciences in Gdańsk, Poland, who started his work on modelling the closely related phenomena of sand compaction, pore pressure generation and soil liquefaction in the early 1980s. His first results in this area were obtained in collaboration with Prof. L. W. Morland from the School of Mathematics of the University of East Anglia in Norwich, UK (Morland and Sawicki 1983, 1985, Sawicki and Morland 1985). Since the mid-1980s, however, for three decades, he worked in this field together with his colleagues from the Institute of Hydro-Engineering in Gdańsk. The results of his work are described in dozens of research papers and a few books devoted to laboratory, theoretical and numerical aspects

of the dynamic behaviour of saturated soils. Many results concerning the sand liquefaction mechanism are summarized in a review paper by Sawicki and Mierczyński (2006) and in a recent book by Sawicki (2014).

In this paper, one of theoretical models developed by Sawicki (1987, 1991) for the description of the process of soil liquefaction is applied to investigate the problem of the dynamic response of saturated sand to seismic loading. This model, due to its formal simplicity, represents a so-called engineering approach to the dynamics of fluid-saturated granular media, as opposed to more rigourous, and thus formally more complex models based on plasticity theories (Mróz et al 1981, Bažant et al 1983, Valanis and Peters 1991). In spite of its simplicity, though, Sawicki's model has proved adequate to describe the key features of the saturated sand behaviour under the passage of seismic waves (Sawicki and Staroszczyk 1995, Staroszczyk 1996)

When investigating the problem of the dynamic behaviour of saturated sands due to seismic waves, interest is usually focused on the analysis of the mechanisms of excess pore pressure generation and soil liquefaction (Gazetas and Yegian 1979, Sawicki and Staroszczyk 1995, Staroszczyk 1996, 1998). That is, internal changes occurring in a saturated soil responding to dynamic loads are studied. The aim of the present paper is to examine how the changes taking place in a saturated sand during its liquefaction affect the characteristics of seismic waves acting on the sand. Hence, the problem of a Rayleigh wave propagation in a water-saturated sand half-space is considered. Assuming that the time-harmonic surface wave has a constant power throughout an earthquake event, it is analysed how the wave properties, such as velocity and length, vary in time as the weakening of the subsoil (due to progressive degradation of its shear strength during the excess pore pressure generation) takes place. Such information on the evolution of the wave parameters during an earthquake can be useful for engineers, as it may enable them to assess the liquefaction hazard for a saturated subsoil.

Equations governing the mechanical behaviour of a water-saturated sand deposit subjected to dynamic loading, together with a description of a sand liquefaction model, are presented in Section 2. In Section 3, a discrete model based on the finite-element method is described. The results of numerical simulations are discussed in Section 4, in which first the process of excess pore pressure build-up and the development of liquefaction zones within the subsoil are illustrated, and then the effects of progressive soil weakening on the variations of free-surface ground displacements and the phase velocity of the surface wave are shown. Concluding remarks are given in Section 5.

2. Formulation of the Problem

The plane-strain surface wave propagation problem in a water-saturated sand deposit is investigated (Fig. 1). It is assumed that the soil occupies the half-space $z \geq 0$ and its elastic material properties are stress-dependent and vary with time t. The medium is

subjected to cyclic loading induced by the passage of time-harmonic Rayleigh waves propagating in the positive x-axis direction.

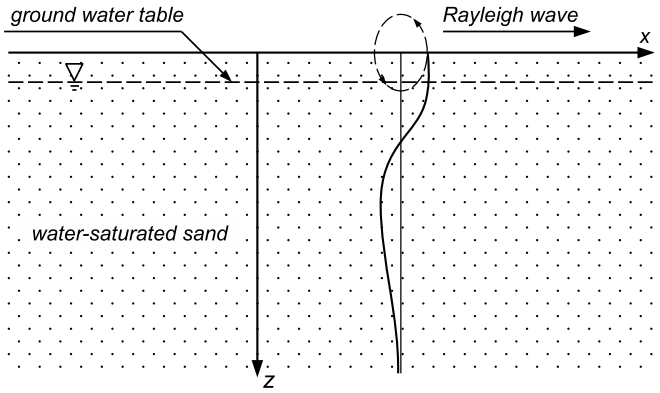

Fig. 1. Plane Rayleigh wave propagation problem definition: coordinate axes and the depth variation of horizontal displacements generated by the passage of a surface wave

The motion of water-saturated sand, which is a two-phase medium, can be described within the framework of Biot's theory of consolidation (Biot 1955) or the theory of mixtures (Bowen 1982). These general theories are based on the assumption that during deformations both constituents of the medium, the soil skeleton and the pore fluid, preserve their independent physical features and separate volumes, all characterized by a single parameter, namely a volume porosity coefficient. Displacement fields in the skeleton and the fluid are described by the vector variables $\boldsymbol{u}^s$ and $\boldsymbol{u}^f$, and partial stress fields in both constituents are defined by the tensor variables $\boldsymbol{\sigma}^s$ and σ^f, with the superscripts s and f referring to the skeleton and the pore fluid, respectively.

In the problem in hand, we deal with a situation in which dynamic loads act over a relatively short period of time, typically not exceeding a minute. Since the phenomenon of soil liquefaction can occur only in saturated sands of low permeability, it can be supposed that no significant drainage of the pore water takes place within such a short period of time. Hence, it can be assumed that no motion of the pore liquid relative to the soil matrix occurs during the ground shaking. That is, the two constituents of the medium can be regarded as moving in unison, so that we have

$$\boldsymbol{u}^s = \boldsymbol{u}^f = \boldsymbol{u}, \tag{1}$$

where $\boldsymbol{u}$ is the displacement vector of the medium treated as a single-phase material.

The total stress $\boldsymbol{\sigma}$ in the water-saturated sand is a sum of partial stresses in its constituents

$$\boldsymbol{\sigma} = \boldsymbol{\sigma}^s + \boldsymbol{\sigma}^f. \tag{2}$$

The pore water is assumed to be an inviscid fluid, and therefore the tensor of the partial stress in the fluid is spherical, that is

$$\boldsymbol{\sigma}^f = -n\, p^f \boldsymbol{I}, \tag{3}$$

where n is the volume porosity of the soil skeleton, p^f is the (intrinsic) pore pressure, and $\boldsymbol{I}$ is the unit tensor. The mechanical behaviour of the soil depends on the effective stress $\boldsymbol{\sigma}'$, defined by

$$\boldsymbol{\sigma}' = \boldsymbol{\sigma} + p^f \boldsymbol{I}. \tag{4}$$

The solid mechanics convention is adopted here, by which positive values of the stress axial components denote tension, whereas positive fluid pressures mean compression.

The bulk soil mass density ρ is defined by intrinsic skeleton and pore fluid densities, ρ^s and ρ^f respectively, by the formula

$$\rho = (1-n)\rho^s + n\rho^f. \tag{5}$$

In terms of the total stress tensor $\boldsymbol{\sigma}$ and the soil density ρ, the equation of motion of the saturated sand, treated as a single-phase material, takes the standard form (Achenbach 1973)

$$\rho\, \ddot{\boldsymbol{u}} = \operatorname{div} \boldsymbol{\sigma} + \rho \boldsymbol{b}, \tag{6}$$

where div denotes the divergence operator, $\boldsymbol{b}$ stands for the body force vector, with the only non-zero component along the z-axis due to gravity, and the superimposed dots denote time differentiation.

During the deformation of the medium, both cyclic and non-cyclic changes occur. Thus, it is convenient to decompose the displacement, strain and stress fields by introducing cyclic (elastic) and non-cyclic (inelastic) parts of these quantities:

$$\begin{aligned} \boldsymbol{u} &= \boldsymbol{u}^C + \boldsymbol{u}^N, \\ \boldsymbol{e} &= \boldsymbol{e}^C + \boldsymbol{e}^N, \\ \boldsymbol{\sigma} &= \boldsymbol{\sigma}^C + \boldsymbol{\sigma}^N, \end{aligned} \tag{7}$$

where $\boldsymbol{e}$ is the infinitesimal strain tensor, with components e_{jk} given in terms of the displacement vector components u_j by the relation

$$e_{jk} = \frac{1}{2}\left(\frac{\partial u_j}{\partial x_k} + \frac{\partial u_k}{\partial x_j}\right), \quad j,k = 1,2, \tag{8}$$

and the superscripts C and N indicate the cyclic and non-cyclic parts of the respective entities. By substituting relations (7) into the linear momentum equation (6), the following two equations can be obtained:

$$\rho\, \ddot{\boldsymbol{u}}^C = \operatorname{div} \boldsymbol{\sigma}^C \tag{9}$$

for cyclic (reversible) variations, and

$$0 = \operatorname{div} \boldsymbol{\sigma}^N + \rho \boldsymbol{b} \tag{10}$$

for non-cyclic (irreversible) variations. The first of the above equations governs the motion of the soil due to dynamic excitations, whereas the second equation describes the stress state due to static loads.

In the problem under consideration, the cyclic motions of the sand deposit are induced by the passage of a time-harmonic Rayleigh surface wave, the action of which, due to its fast exponential decay with increasing depth z, is essentially confined to the region close to the ground free surface. For a surface wave propagating in the positive x-direction, the general solution of equation (9) for cyclic motions of the soil can be expressed in the form (Achenbach 1973):

$$\boldsymbol{u}^C(x, z, t) = \boldsymbol{C}(z) \exp[i(\omega t - kx)], \tag{11}$$

where ω is the angular frequency of oscillations, $i = \sqrt{-1}$ is the imaginary unit, and k is the wave number. The function $\boldsymbol{C}(z)$ describes the depth-displacement profile of the wave. This function is determined by boundary conditions that must be satisfied by stress components at the traction-free surface $z = 0$, and by the condition that displacements must vanish at $z \to \infty$.

Time-harmonic variations of the cyclic parts of the displacement, strain and stress fields can be expressed by their amplitudes. Thus,

$$\begin{aligned} \boldsymbol{u}^C &= \boldsymbol{U} \exp(i\omega t), \\ \boldsymbol{e}^C &= \boldsymbol{E} \exp(i\omega t), \\ \boldsymbol{\sigma}^C &= \boldsymbol{T} \exp(i\omega t), \end{aligned} \tag{12}$$

where the quantities $\boldsymbol{U}$, $\boldsymbol{E}$ and $\boldsymbol{T}$ denote, respectively, the amplitudes of the displacement vector, strain tensor and stress tensor.

It is assumed that the cyclic components of the sand deformation are due to the elastic response of the medium. Thus, a linear Hooke's law is adopted to describe the elastic behaviour of the saturated sand:

$$\boldsymbol{\sigma}^C = \lambda \operatorname{tr}(\boldsymbol{e}^C) \boldsymbol{I} + G \boldsymbol{e}^C, \tag{13}$$

where λ and G are Lamé's elastic constants. Both elastic parameters are assumed to be dependent on the effective stress in the soil (that is, they vary during the process of pore pressure development). The stress-dependence of the shear modulus G is described by a relation due to Hardin and Drnevich (1972), based on experimental measurements; that is

$$G = G_0 + G_1 \sqrt{\frac{p'}{p^*}}\,, \tag{14}$$

where G_0 and G_1 are measured material parameters, p' denotes the mean effective stress in the solid, and $p^* = 10^5$ Pa is a normalizing stress unit. The quantity p' is defined by

$$p' = \frac{1}{3}\,\mathrm{tr}(\boldsymbol{\sigma}^N) - p^f, \tag{15}$$

where $\mathrm{tr}(\cdot)$ denotes the trace operator. The first term on the right-hand side of equation (15) denotes the mean total stress in the soil due to static (non-cyclic) loading. Because of the lack of empirical data regarding the dependence of λ on p', it is assumed here that the latter elastic parameter is determined from the condition that the Poisson ratio ν remains constant during the soil deformation under seismic loads.

The non-cyclic strain $\boldsymbol{e}^N$, entering equation $(7)_2$, can be divided into two parts:

$$\boldsymbol{e}^N = \boldsymbol{e}^S + \boldsymbol{e}^\Phi, \tag{16}$$

where $\boldsymbol{e}^S$ denotes a static part of the tensor $\boldsymbol{e}^N$ and represents the settlement of the soil under its own weight. The strain $\boldsymbol{e}^S$, together with the corresponding stress $\boldsymbol{\sigma}^N$ appearing in equation (15), can be easily found by standard methods of the classical soil mechanics.

The tensor $\boldsymbol{e}^\Phi$ in equation (16) represents strains which develop in the sand during cyclic shearing and are caused by irreversible rearrangements in the granular structure of the soil. In order to determine these strains, the engineering compaction theory proposed by Sawicki (1987, 1991) is applied. This theory can be regarded as a simplified version of the earlier, more rigourous, formulations by Morland and Sawicki (1983, 1985), based on the mixture theory for compaction of granular materials. The theory stems from two observations: (1) soil compaction, meant as a progressive decrease in the soil volume due to irreversible changes in its internal structure, depends on the magnitudes of shear strains, and (2) the rate of compaction decreases with increasing magnitude of the current compaction. In the simplified approach Sawicki (1987, 1991) the behaviour of the compacting sand is averaged over each cycle of loading, and the interest is restricted to the mean trend; that is, the local oscillations imposed on this trend are neglected. Hence, the constitutive law governing sand compaction is expressed as

$$\frac{\partial \Phi}{\partial N} = D_1 J \exp\left(-D_2 \Phi\right), \tag{17}$$

where Φ is the sand compaction measure and N is the number of cycles, treated as a continuous variable. J denotes the second invariant of the deviatoric part of the strain amplitude tensor $\boldsymbol{E}$; thus

$$J = \frac{1}{2}\,\mathrm{tr}\left(\boldsymbol{E}'\right)^2, \tag{18}$$

where

$$\boldsymbol{E}' = \boldsymbol{E} - \frac{1}{3}\,\mathrm{tr}(\boldsymbol{E})\boldsymbol{I}. \tag{19}$$

The parameters D_1 and D_2 in the compaction law (17) are material constants of a given sand, and can be measured experimentally.

Equation (17) describes the behaviour of saturated sand under free-draining conditions, in which the fluid can filtrate through the pores as the soil compaction occurs. In undrained conditions, however, the rearrangement of soil grains is resisted by the pore fluid, and, consequently, pore pressures in excess of their hydrostatic values are generated. The mechanisms of sand compaction in free-draining conditions and pore pressure generation in undrained conditions can be quantitatively related to each other by the formula proposed by Martin et al (1975) on empirical basis:

$$\frac{\partial s}{\partial N} = \frac{1}{\alpha}\,\frac{\partial \Phi}{\partial N}, \tag{20}$$

in which s denotes the excess pore pressure and α is a material constant defined by

$$\alpha = \frac{1-n}{n}\,\kappa, \tag{21}$$

where κ is the soil skeleton compressibility.

Simultaneously with the generation of excess pressures in the pore water, the process of pore pressure dissipation also takes place, caused by the vertical pressure gradients in the fluid. The equation governing this dissipation mechanism, assuming pore fluid incompressibility, has the form (Verruijt 1969):

$$\frac{\partial s}{\partial t} = \beta\,\nabla^2 s, \tag{22}$$

with the coefficient β defined by

$$\beta = \frac{k_f}{\rho^f \kappa}, \tag{23}$$

and ∇^2 denoting the Laplace operator. The filtration equation (22) is solved with the following boundary conditions:

$$s(x, h_w, t) = 0, \quad \lim_{z\to\infty} \frac{\partial s}{\partial z} = 0, \tag{24}$$

where h_w is the depth of the ground water table. The second of the latter equations means that there is no pore water flow at the infinite depth z.

The solution of the system of three equations (17), (20) and (22) with relevant initial and boundary conditions describes the evolution of pore pressures with the increasing number of loading cycles N. The increasing pore pressure s gradually reduces the mean effective stress p' in the soil. Assuming that at the start of cyclic loading we have

$$p'(N=0) = p'_0\,, \quad s(N=0) = 0, \tag{25}$$

where p'_0 is the initial (static) mean effective stress, the changes in p' can be expressed by

$$p' = p'_0 - s. \tag{26}$$

As follows from equations (26) and (14), the increasing excess pore pressure s progressively reduces the shear resistance of the saturated sand, until the state $p' = 0$ is reached and the soil shear modulus G decreases to its residual value G_0. As soon as the condition $p' = 0$ is reached at a given point in the soil, the latter is said to have liquefied at this point. It is supposed here that after the onset of liquefaction no further generation of the excess pore pressure occurs at a given point, and the shear modulus, of the value G_0, remains constant afterwards (the mechanism of soil re-solidification is not considered in this analysis).

3. Discrete Solution Method

The plane wave propagation problem was solved by employing a finite-element method in space variables and an incremental step-by-step method in time. For computational purposes, the semi-infinite sand domain was replaced by a layer of finite thickness H (see Fig. 2); such a replacement can be performed as long as H is sufficiently large compared to the surface wave length L_R. A rigid base at the bottom $z = H$ of the sand layer was adopted, with zero horizontal and vertical sand displacements assumed there. In the simulations, the results of which are illustrated in Section 4, the layer depth H was assumed to be equal to about two initial surface wave lengths ($H \sim 2L_R$). A mesh of rectangular finite elements was imposed on the sand layer, with the element uniform horizontal dimensions a and variable dimensions b_j ($j = 1, \ldots, m$) along the vertical direction, where m denotes the number of finite elements across the depth of the computational layer.

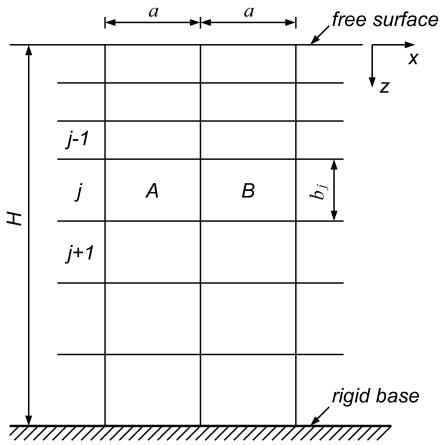

Fig. 2. Discretization of a water-saturated sand domain

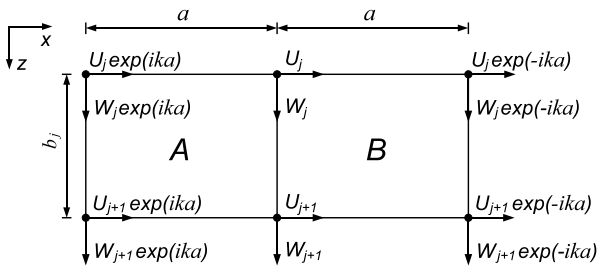

Fig. 3. Two adjacent rectangular finite elements A and B shown in Fig. 2

The plane problem of time-harmonic surface waves propagating along the x-axis can be reduced to a one-dimensional in space by applying a method proposed by Lysmer (1970), and subsequently employed by Sawicki and Staroszczyk (1995) and Staroszczyk (1996). To outline the idea of Lysmer's method, let consider a pair of two adjacent finite elements (see Fig. 3), lying in the same, say j-th, discrete sublayer. As follows from equation (11), describing the propagation of a surface wave in the positive x-axis direction, the horizontal displacement amplitudes $U(x,z)$ at nodal points situated at the same depth z are related to each other by the formulae

$$\begin{aligned} U(x-a,z) &= U(x,z)\exp(ika), \\ U(x+a,z) &= U(x,z)\exp(-ika). \end{aligned} \tag{27}$$

Obviously, analogous relations apply to the vertical displacement amplitudes $W(x,z)$. Expressions (27) determine the displacement amplitudes at three adjacent discrete nodes spaced by a in the horizontal direction as: $U_j \exp(ika)$, U_j and $U_j \exp(-ika)$, and, similarly, for the vertical displacement amplitudes as: $W_j \exp(ika)$, W_j and $W_j \exp(-ika)$. Hence, the displacement amplitudes at all nodes of the two adjacent elements A and B, shown in Fig. 3, are uniquely determined by the amplitudes U_j, W_j, U_{j+1} and W_{j+1}, defining the medium motions within the j-th discrete sublayer of thickness b_j.

Let the nodal displacement amplitudes for the j-th sublayer be listed in a four--element vector $\boldsymbol{q}_j$

$$\boldsymbol{q}_j = \left(U_j, W_j, U_{j+1}, W_{j+1}\right)^T, \tag{28}$$

where the superscript T denotes vector transposition. Similarly, the corresponding four nodal force amplitudes at the j-th discrete sublayer can be listed in a vector $\boldsymbol{Q}_j$. Then, the dependence between the nodal forces and displacement amplitudes in the j-th sublayer can be expressed in the form

$$\boldsymbol{Q}_j = \boldsymbol{K}_j\, \boldsymbol{q}_j\,, \tag{29}$$

where $\boldsymbol{K}_j$ is a complex-valued 4×4 stiffness matrix of the j-th sublayer. The elements of this matrix are functions of the elastic constants G_j and λ_j, the dimensions a and

b_j, and the surface wave number k. In an analogous manner, the relationship between the four nodal inertia forces and acceleration amplitudes can be derived, with the j-th sublayer mass matrix $\boldsymbol{M}_j$ given in terms of the density ρ_j of the j-th sublayer and the finite element dimensions a and b_j. The matrix $\boldsymbol{M}_j$, as opposed to $\boldsymbol{K}_j$, is a real matrix.

It is known that the smaller the finite element dimensions are, the better is the discrete approximation of the continuous medium. Therefore, it seems reasonable to choose the horizontal element size a as small as possible, that is, to calculate the sublayer mass and stiffness matrices for $a \to 0$. All relevant details concerning the limit mass and stiffness matrices, including the definitions of their entries, can be found in the paper by Staroszczyk (1996). Here we only note that by assembling the global mass and stiffness matrices from the corresponding limit sublayer matrices in a way typical of the finite-element method (Zienkiewicz et al 2005), the wave propagation problem under consideration is reduced to the solution of the following matrix equation:

$$\left(\boldsymbol{K} - \omega^2 \boldsymbol{M}\right) \boldsymbol{q} = \boldsymbol{O}. \tag{30}$$

In (30), $\boldsymbol{M}$ and $\boldsymbol{K}$ denote, respectively, the global mass and stiffness matrices, and $\boldsymbol{q}$ is the global displacement amplitude vector (containing displacement amplitudes at all discrete nodes across the soil vertical profile), and $\boldsymbol{O}$ is the zero vector.

Equation (30) defines a generalized eigenvalue problem for the complex matrix $\boldsymbol{K}$ and the real tri-diagonal matrix $\boldsymbol{M}$. Since the angular frequency ω is a prescribed parameter, the solution of (30) yields a set of eigenvalues which are the wave numbers $k_r (r = 1, \ldots, 2m)$, together with the corresponding set of $2m$ eigenvectors $\boldsymbol{q}_r$. The lowest (fundamental) eigenvalue, k, corresponds to the wave number of the surface wave, with its phase velocity given by $c_R = \omega/k$ and its length given by $L_R = 2\pi/k$. The eigenvector corresponding to the lowest eigenvalue, the so-called fundamental Rayleigh mode, determines the variation of soil displacement amplitudes with depth z. This fundamental mode is normalized by means of a chosen wave parameter (for instance, the free-surface displacement or acceleration amplitude) in order to represent a physical wave. The remaining $2m - 1$ eigenvalues (wave numbers) and eigenvectors (wave modes) are discarded from the analysis, since they represent standing waves which appear in the discrete solution because the layer of finite thickness H is considered instead of a semi-infinite half-space.

The above procedure is repeated at each incremental step of calculations throughout the whole time of a numerical simulation. At each step, depending on current displacement, deformation and stress fields in the soil, the material constants G and λ are updated accordingly to reflect the gradual weakening of the strength of the medium as soil liquefaction progresses.

4. Numerical Illustrations

Numerical simulations were carried out for soil material parameters corresponding to medium-dense Ottawa sand. Hence, the following data were adopted: $G_0 = 10$ MPa

and $G_1 = 70$ MPa for shear moduli, $n = 0.4$ for the volume porosity, $\nu = 0.25$ for the Poisson ratio (this value implies that $\lambda = G$), $\rho^s = 2650$ kg/m^3 for the intrinsic sand density, and $K_0 = 0.5$ for the earth pressure coefficient (needed to calculate mean stresses in the soil due to its own weight). The depth of the ground water table was assumed as $h_w = 2$ m below the ground free surface. The parameters $D_1 = 1740$ and $D_2 = 115$ (Sawicki 1991) were used in the sand compaction law (17). The discrete model described in Section 3 has the computational depth $H = 200$ m, and consisted of 200 discrete sublayers, with the upper 100 of thickness 0.5 m each.

The results presented below have been obtained for a Rayleigh surface wave of frequency $f_R = 2$ Hz (corresponding to the wave period $T = 0.5$ s and the angular frequency $\omega = 12.57$ s^{-1}). For the adopted material parameters of the soil, the initial (that is before the liquefaction starts) phase velocity of the surface wave is equal to about 214 m/s (which for the wave period $T = 0.5$ s gives the wave length $L_R = 107$ m — this is about a half of the computational domain depth). It was assumed in the simulations that during each cycle of the ground shaking the mechanical power of the surface waves remains constant. The consequence of this simplification is that when the subsoil weakens (due to a decrease in effective pressures) then displacements and strains increase in the medium. The simulations were conducted for earthquake events lasting for 30 seconds. The main goal was to investigate the effects of the sand filtration coefficient k_f and the magnitude of the initial ground vertical acceleration amplitude a_0^V on the dynamic behaviour of the subsoil. Basically, the cases of k_f varying between 10^{-6} and 10^{-3} m/s, and of a_0^V varying between 0.05 and 0.20 g were examined.

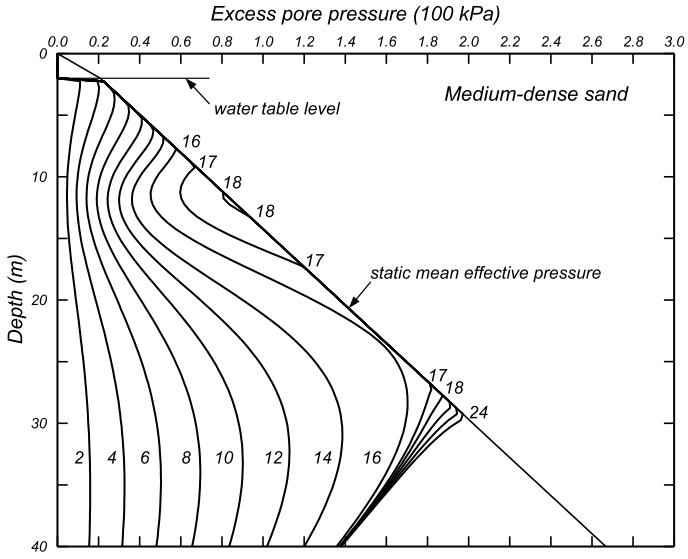

Fig. 4. History of excess pore pressure generation in a water-saturated sand half-space. The labels of the curves indicate time in seconds. ($a_0^V = 0.1\,g$, $k_f = 10^{-6}$ m/s)

Figure 4 illustrates the history of excess pore pressure generation in a water-saturated sand deposit for which the filtration coefficient has the value $k_f = 10^{-6}$ m/s. The results presented have been obtained for a surface wave producing free-surface vertical motions of the amplitude $a_0^V = 0.1\,g$ in the first cycle of shaking. In the figure, the numbers by respective depth profiles indicate the time in seconds corresponding to these curves.

It can be seen that the most rapid increase in excess pore pressures occurs at depths of about 25 to 30 m; that is, approximately at a depth $0.25\,L_R$ (a quarter of the Rayleigh wave length). One can observe that the most dramatic development of sand liquefaction takes place within 16 to 18 s, when the whole layer between 10 and 25 m liquefies. This is in contrast to the situation occurring immediately under the water table, where liquefaction develops steadily at an approximately constant rate.

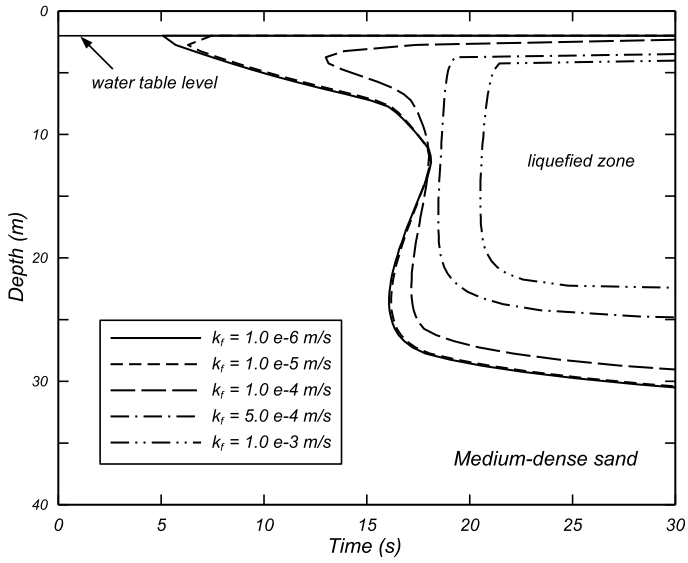

Fig. 5. Development of liquefaction zones in water-saturated sand for different values of the filtration coefficient k_f ($a_0^V = 0.1\,g$)

Corresponding to the previous figure are the plots in Figure 5, showing the development in time of the zones of liquefied sand. The plots, obtained for a surface wave producing the ground shaking of the initial acceleration amplitude $a_0^V = 0.1\,g$, illustrate the influence of the soil permeability on the liquefaction process. It was found that the only values of interest are those of the filtration coefficient in the range 10^{-6} m/s $\lesssim k_f \lesssim 10^{-3}$ m/s. For smaller values, the response of the sand is practically unchanged with decreasing k_f, whereas for the values of $k_f \gtrsim 10^{-3}$ m/s no liquefaction occurs (naturally, for the adopted soil and surface wave parameters). It can be noted that for more permeable sands no liquefaction takes place immediately under the water table (due to the fast dissipation of excess pressures there). On the other

hand, once liquefaction starts, it abruptly (within around one second) involves a thick layer of the sand.

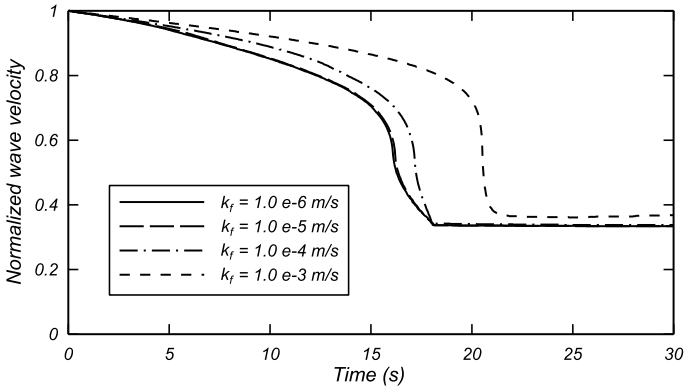

Fig. 6. Time variation of normalized Rayleigh wave velocity as a function of the filtration coefficient k_f, for the initial free-surface vertical acceleration amplitude $a_0^V = 0.1\ g$

Figures 6 to 9 illustrate the time variation of the Rayleigh wave velocity and the free-surface displacement components. These are quantities which can be directly measured during an earthquake, and the analysis of their time-changes can provide some information on the state of the subsoil deep under the ground level (for instance, whether it has liquefied or not). The first two figures show the variation of surface wave velocities. The velocities c_R are normalized by means of the initial wave speed c_R^0 at the beginning of an earthquake, before any internal changes in the subsoil have occurred. Fig. 6 demonstrates the effect of the soil permeability on the wave velocity. By comparing the plots in this figure with those in Fig. 5, one can easily see that the instants of dramatic changes in the wave speed for different soil filtration coefficients are exactly correlated with the instants at which large regions of the subsoil are liquefied within a short period of time. The plots shown in Fig. 7 display the effect of the strength of an earthquake on the time variations of the surface wave velocity. Hence, the results for different acceleration amplitudes a_0^V of the initial ground vertical motions are compared (for $k_f = 10^{-6}$ m/s). It is seen that the effect of a_0^V on the soil dynamic response is considerable. While for a_0^V as small as $0.05\ g$ the decrease in wave velocity (that is, the decrease in the strength of the subsoil) is quite small after 30 s, for larger values of a_0^V, $0.15\ g$ and $0.20\ g$, a very rapid degradation of the subsoil strength is visible, with the liquefaction process completed within around 5 s in the case of the latter value.

Finally, in Figures 8 and 9 the time variations of the free-surface soil displacement amplitudes U and W are illustrated. These amplitudes are normalized with respect to the initial vertical displacement amplitude $W_0 = W(z = 0, t = 0)$ at the start of the ground shaking; that is, the quantities $U(z = 0, t)/W_0$ and $W(z = 0, t)/W_0$ are displayed in the plots. In the first of these figures, the histories of the vertical components of the

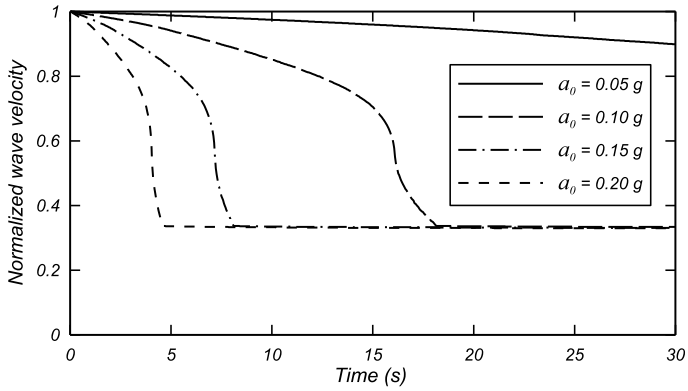

Fig. 7. Time variation of normalized Rayleigh wave velocity as a function of the initial free-surface vertical acceleration amplitude a_0^V, for the filtration coefficient $k_f = 10^{-6}$ m/s

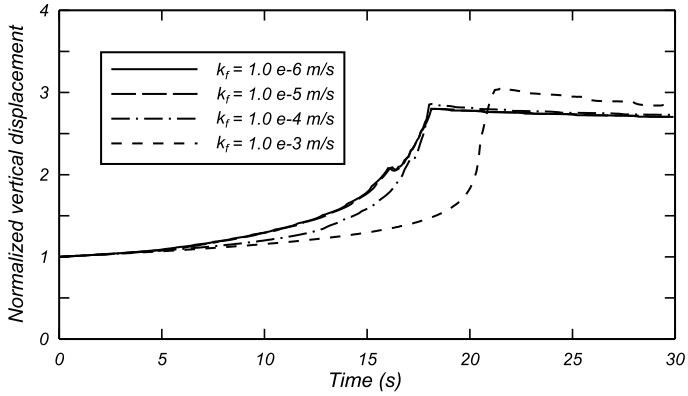

Fig. 8. Time variation of normalized free-surface vertical displacement amplitudes as a function of the sand filtration coefficient k_f, for the initial free-surface vertical acceleration amplitude $a_0^V = 0.1\,g$

free-surface displacement amplitudes are shown for different soil filtration coefficient values k_f, and in the second figure the histories of the horizontal components are depicted. One can note that the increase in vertical displacements with the progressive weakening of the subsoil is much larger than that in horizontal displacements. The vertical amplitude components (Fig. 8) are seen to vary roughly regularly and first increase gradually until the full development of liquefaction in the subsoil, and then slightly decrease. On the other hand, the horizontal free-surface displacements (Fig. 9) initially grow smoothly, but prior to the start of extensive liquefaction undergo irregular variations, before they slightly decrease after the liquefaction in the subsoil has fully developed.

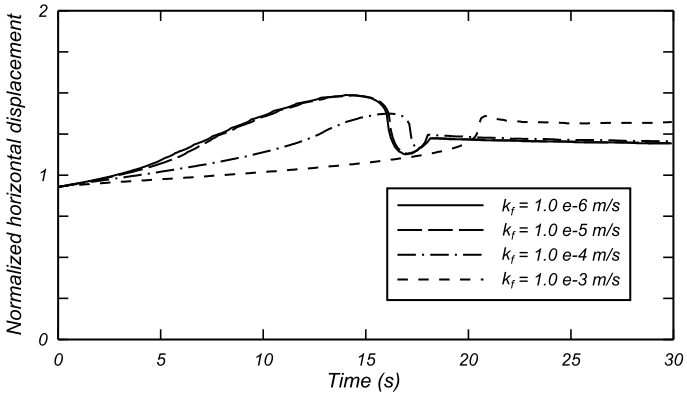

Fig. 9. Time variation of normalized free-surface horizontal displacement amplitudes as a function of the sand filtration coefficient k_f, for the initial free-surface vertical acceleration amplitude $a_0^V = 0.1\,g$

5. Conclusions

In this paper, the problem of the dynamic response of a water-saturated sand deposit to loads induced by the passage of a Rayleigh surface wave was investigated. The emphasis was placed on the mechanism of soil liquefaction and its effect on the evolution of surface wave characteristics during the progressive weakening of the subsoil.

It was found that, for ground motions of vertical acceleration amplitudes of order $0.1\,g$, an extensive liquefaction zone can develop in a saturated medium-dense sand within less than twenty seconds from the onset of ground shaking. Liquefaction is an abrupt process, since most of the saturated sand becomes liquefied within a period of about two seconds. Surprisingly, sands with higher permeability liquefy more violently (though obviously the process starts later in them) than those which are less permeable.

The weakening of the soil caused by the generation of excess pore pressures is reflected by the changes in the phase velocity of the surface wave, with the most dramatic variations occurring prior to and during the abrupt expansion of the region of liquefied sand. Assuming that the surface wave power remains unchanged during the shaking, it was found that free-surface sand displacements undergo significant changes. The amplitudes of vertical ground motions steadily increase until the liquefaction has fully developed, and then slightly decrease over time. The amplitudes of horizontal ground motions also increase until the liquefaction process is completed, but at smaller rates than the vertical components. After reaching this stage, the horizontal ground motions also slightly decrease. This small decrease in both components of the free-surface displacements is the consequence of the redistribution of excess pore pressures in the soil due to the pressure dissipation process.

References

Achenbach J. D. (1973) *Wave Propagation in Elastic Solids*, North-Holland, Amsterdam.

Bažant Z. P., Krizek R. J. and Shieh C. L. (1983) Histeretic endochronic theory for sand, *Proc. ASCE, J. Eng. Mech.*, **109** (4), 1073–1095.

Biot M. A. (1955) Theory of elasticity and consolidation for a porous anisotropic solid, *J. Appl. Phys.*, **26** (2), 182–185.

Bowen R. M. (1982) Compressible porous media models by use of the theory of mixtures, *Int. J. Eng. Sci.*, **20** (6), 697–735.

Finn W. D. L., Lee K. W. and Martin G. R. (1977) An effective stress model for liquefaction, *Proc. ASCE, J. Geotech. Eng. Div.*, **103** (6), 517–533.

Finn W. D. L., Pickering D. J. and Bransby P. L. (1971) Sand liquefaction in triaxial and simple shear tests, *Proc. ASCE, J. Soil Mech. Found. Div.*, **97** (4), 639–659.

Gazetas G. and Yegian M. K. (1979) Shear and Rayleigh waves in soil mechanics, *Proc. ASCE, J. Geotech. Eng. Div.*, **105**, 1455–1470.

Hardin R. and Drnevich V. P. (1972) Shear modulus and damping in soils: measurement and parameter effects, *Proc. ASCE, J. Soil Mech. Found. Div.*, **98** (6), 603–624.

Lysmer J. (1970) Lumped mass method for Rayleigh waves, *Bull. Seism. Soc. Am.*, **60** (1), 89–104.

Martin G. R., Finn W. D. L. and Seed H. B. (1975) Fundamentals of liquefaction under cyclic loading, *Proc. ASCE, J. Geotech. Eng. Div.*, **101**, 423–438.

Morland L. W. and Sawicki A. (1983) A mixture model for the compaction of saturated sand, *Mech. Mater.*, **2** (3), 203–216.

Morland L. W. and Sawicki A. (1985) A model for compaction and shear hysteresis in saturated granular materials, *J. Mech. Phys. Solids*, **33**, 1–24.

Mróz Z., Norris V. A. and Zienkiewicz O. C. (1981) An anisotropic, critical state model for soils subject to cyclic loading, *Gèotechnique*, **31** (4), 451–469.

Sawicki A. (1987) An engineering model for compaction of sand under cyclic loading, *Eng. Trans.*, **35** (4), 677–693.

Sawicki A. (1991) *Mechanics of Soils under Cyclic Loading* (in Polish), IBW PAN Publishing House, Gdańsk.

Sawicki A. (2014) *The Puzzle of Soil Liquefaction*, IBW PAN Publishing House, Gdańsk.

Sawicki A. and Mierczyński J. (2006) Developments in modeling liquefaction of granular soils, caused by cyclic loads, *Appl. Mech. Rev.*, **59** (2), 91–106.

Sawicki A. and Morland L.W. (1985) Pore pressure generation in a saturated sand layer subjected to a cyclic horizontal acceleration at it base, *J. Mech, Phys. Solids*, **33** (6), 545–559.

Sawicki A. and Staroszczyk R. (1995) Development of ground liquefaction due to surface waves, *Arch. Mech.*, **47** (3), 557–576.

Seed H. B. and Lee K. L. (1966) Liquefaction of saturated sands during cyclic loading, *Proc. ASCE, J. Soil Mech. Found. Div.*, **92** (6), 105–134.

Seed H. B. and Peacock W. H. (1971) Test procedures for measuring soil liquefaction characteristics, *Proc. ASCE, J. Soil Mech. Found. Div.*, **97** (8), 1099–1119.

Staroszczyk R. (1996) Pore pressure generation and liquefaction in saturated sands due to the propagation of surface waves, *Acta Geophys. Pol.*, **44** (2), 195–218.

Staroszczyk R. (1998) Love wave-induced liquefaction in a saturated sand layer, *J. Theor. Appl. Mech.*, **36** (3), 723–744.

Valanis K. C. and Peters J. F. (1991) An endochronic plasticity theory with shear-volumetric coupling, *Int. J. Numer. Anal. Meth. Geomech.*, **15** (2), 77–102, DOI: 10.1002/nag.1610150202.

Verruijt A. (1969) Elastic storage of aquifers, in: *Flow through Porous Media* (ed. R. J. M. De Wiest), chap. 8, Academic Press, New York, pp. 331–376.

Zienkiewicz O. C., Taylor R. L. and Zhu J. Z. (2005) *The Finite Element Method: Its Basis and Fundamentals*, Elsevier Butterworth-Heinemann, Amsterdam, 6th edn.